Slovak Society of Chemical Engineering
Institute of Chemical and Environmental Engineering
Slovak University of Technology in Bratislava

PROCEEDINGS

52nd International Conference of the Slovak Society of Chemical Engineering SSCHE 2026

Hotel SOREA TRIGAN
Štrbské Pleso, Slovakia
May 26 - 29, 2026

Editors: Assoc. prof. Mário Mihaľ

ISBN: 978-80-8208-177-3, EAN: 9788082081773

Published by the Faculty of Chemical and Food Technology, Slovak University of Technology in Bratislava in Slovak Chemistry Library for the Institute of Chemical and Environmental Engineering; Radlinského 9, 812 37 Bratislava, 2026

KARAKUŞ, N., SERDAROĞLU, G.: Electronic Structure and Reactivity Descriptors of BN-Doped Naphthalimide-Carbazole Bipolar OLED Emitters: A DFT/TD-DFT Study, Editors: Mihaľ, M., In *52nd International Conference of the Slovak Society of Chemical Engineering SSCHE 2026*, Štrbské Pleso, Slovakia, 2026.

Electronic Structure and Reactivity Descriptors of BN-Doped Naphthalimide–Carbazole Bipolar OLED Emitters: A DFT/TD-DFT Study

Nihat Karakuş[1], Goncagül Serdaroğlu[2]

[1]*Sivas Cumhuriyet University, Faculty of Science, Department of Chemistry, Sivas, Türkiye*
[2]*Sivas Cumhuriyet University, Faculty of Education, Department of Mathematics and Science Education, Sivas, Türkiye*

e-mail: nkarakus@cumhuriyet.edu.tr

Abstract

Organic light-emitting diode (OLED) technologies depend on precise control of molecular electronic structure to enable efficient charge transport and stable emission. In this context, naphthalimide–carbazole-based bipolar emitters offer a versatile donor–acceptor framework for tuning optoelectronic properties. The molecular structures studied include three reference compounds (1–3), where carbazole and triphenylamine units act as electron-donating segments, and the naphthalimide core functions as the electron-accepting unit. A boron–nitrogen (BN) isosteric doping strategy is applied to these structures to systematically explore changes in electronic properties. BN units are selectively incorporated into the acceptor core and nearby aromatic regions, adjusting the distribution of frontier molecular orbitals while maintaining the overall π-conjugated framework of the parent molecules. Density functional theory (DFT) and time-dependent DFT (TD-DFT) calculations are used to assess key electronic features, including HOMO–LUMO energy levels, global reactivity descriptors, and molecular electrostatic potential (MEP) maps. The findings show that structural differences among compounds 1–3, especially in donor strength and substitution patterns, significantly impact orbital localization and charge distribution. Comparing these results reveals that BN substitution further enhances electronic polarization and influences donor–acceptor interactions based on the substitution site. These outcomes highlight that both the molecular architecture and BN-doping strategy are crucial in shaping electronic behavior. Overall, this study offers a structure-based computational perspective on BN-doped naphthalimide–carbazole systems and provides guiding principles for designing efficient bipolar OLED emitter materials.

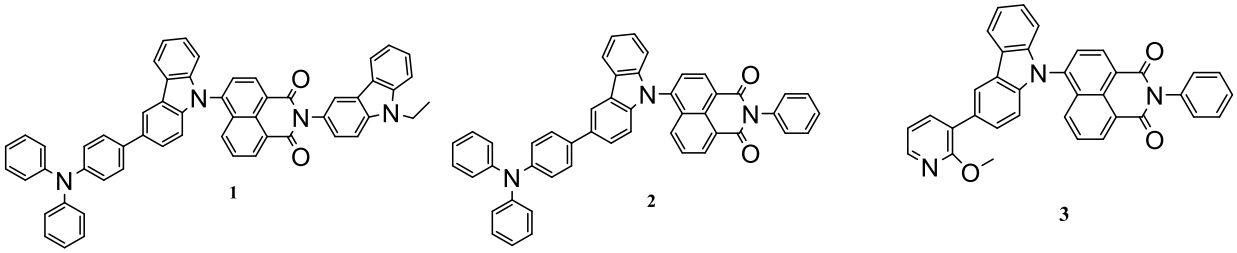

Key words: OLED, BN-doping, bipolar emitters, TADF, DFT

References

[1] Kumar A, Lenka S, Patidar K, Tung CA, Luo MY, Beresneviciute R, Grigalevicius S (2026) Molecules. 31(1): 158.

[2] Masimukku N, et al. (2022) Phys Chem Chem Phys. 24: 5070–5082.

[3] otowicz S, Korzec M, Pająk AK, Golba S, Małecki JG, Siwy M, et al. (2021) Materials. 14(11): 2714.

[4] Chen C, Zhang Y, Wang XY, Wang JY, Pei J (2023) Chem Mater. 35: 10277–10294.

[5] Lee C, Yang W, Parr RG (1988) Phys Rev B. 37: 785–789.

[6] Parr RG, Szentpaly LV, Liu S (1999) J Am Chem Soc. 121: 1922–1924.

[7] Adachi C (2014) Jpn J Appl Phys. 53: 060101.

[8] Wong MY, Zysman-Colman E (2017) Adv Mater. 29: 1605444.

[9] Yang Z, Mao Z, Xie Z, et al. (2017) Chem Soc Rev. 46: 915–1016.

[10] Runge E, Gross EKU (1984) Phys Rev Lett. 52: 997–1000.

[11] Frisch MJ, Trucks GW, Schlegel HB, et al. (2019) Gaussian 16, Revision C.01. Gaussian Inc., Wallingford CT.

Electronic Structure and Reactivity Descriptors of BN-Doped Naphthalimide–Carbazole Bipolar OLED Emitters: A DFT/TD-DFT Study

Nihat Karakuş [*,1], Goncagül Serdaroğlu [2]

[1]*Sivas Cumhuriyet University, Faculty of Science, Department of Chemistry, 58140 Sivas, Turkey; e-mail: nkarakus@cumhuriyet.du.tr*

[2]*Sivas Cumhuriyet University, Faculty of Education, Math. and Sci. Edu., 58140, Sivas, Turkey; e-mail: goncagul.serdaroglu@gmail.com*

**Corresponding Author: [1]Sivas Cumhuriyet University, Faculty of Science, Department of Chemistry, 58140 Sivas, Turkey; e-mail: nkarakus@cumhuriyet.du.tr*

Abstract

Organic light-emitting diode (OLED) technologies depend on precise control of molecular electronic structure to enable efficient charge transport and stable emission. In this context, naphthalimide–carbazole-based bipolar emitters offer a versatile donor–acceptor framework for tuning optoelectronic properties. The molecular structures studied include three reference compounds (1–3), where carbazole and triphenylamine units act as electron-donating segments, and the naphthalimide core functions as the electron-accepting unit. A boron–nitrogen (BN) isosteric doping strategy is applied to these structures to systematically explore changes in electronic properties. BN units are selectively incorporated into the acceptor core and nearby aromatic regions, adjusting the distribution of frontier molecular orbitals while maintaining the overall π-conjugated framework of the parent molecules. Density functional theory (DFT) and time-dependent DFT (TD-DFT) calculations are used to assess key electronic features, including HOMO–LUMO energy levels, global reactivity descriptors, and molecular electrostatic potential (MEP) maps. The findings show that structural differences among compounds 1–3, especially in donor strength and substitution patterns, significantly impact orbital localization and charge distribution. Comparing these results reveals that BN substitution further enhances electronic polarization and influences donor–acceptor interactions based on the substitution site. These outcomes highlight that both the molecular architecture and BN-doping strategy are crucial in shaping electronic behavior. Overall, this study offers a structure-based computational perspective on BN-doped naphthalimide–carbazole systems and provides guiding principles for designing efficient bipolar OLED emitter materials

Keywords: *OLED, BN-doping, bipolar emitters, TADF, DFT*

1. Introduction

Organic light-emitting diodes (OLEDs) have emerged as a key technology in modern optoelectronic applications due to their high efficiency, flexibility, and tunable emission properties [1-3]. The performance of OLED devices is fundamentally governed by the electronic structure of the emissive materials, particularly the alignment of frontier molecular orbitals and the balance between electron-donating and electron-accepting units [4, 5]. In this context, bipolar donor–acceptor systems based on naphthalimide–carbazole frameworks have attracted considerable attention for their ability to enable balanced charge transport and controlled emission behavior [6-8]. Naphthalimide derivatives act as strong electron-accepting cores, while carbazole and

triphenylamine units serve as efficient electron donors, forming a well-defined intramolecular charge-transfer system. Naphthalimide derivatives act as strong electron-accepting cores, while carbazole and triphenylamine units serve as efficient electron donors, forming a well-defined donor–π–acceptor (D–π–A) architecture that promotes intramolecular charge transfer. In this framework, the π-bridge serves as an electronic conduit, comprising conjugated aromatic linkers that connect the donor units to the naphthalimide acceptor core. This π-conjugated pathway enables efficient electronic communication between spatially separated frontier orbitals, facilitating charge delocalization and tuning the extent of donor–acceptor coupling. As a result, the electronic distribution, optical transitions, and overall device-relevant properties can be precisely modulated through structural variations within the π-bridge and substituent positioning. Such controllable D–π–A interactions are therefore central to optimizing charge transport balance, emission efficiency, and overall performance in OLED systems.

In this context, boron–nitrogen (BN) isosteric substitution emerges as a powerful molecular engineering strategy to fine-tune these interactions further. By selectively incorporating BN units into the π-bridge and acceptor segments, it becomes possible to modulate electronic polarization, adjust frontier orbital localization, and control donor–acceptor coupling without disrupting the overall π-conjugated framework. This position-dependent electronic perturbation provides an additional degree of freedom for tailoring optoelectronic properties, thereby offering a rational pathway for optimizing the performance of bipolar OLED emitters. The modulation of this donor–acceptor interaction plays a crucial role in determining the electronic distribution, optical response, and overall device efficiency [9-14]. In particular, donor–acceptor (D–A) molecular architectures are widely recognized as effective platforms for achieving balanced charge injection and transport, enabling high external quantum efficiency (EQE) and long device lifetime in OLED systems (15, 16]. Therefore, rational molecular design strategies that can precisely tune the electronic structure without disrupting the π-conjugated framework are of significant importance. Boron–nitrogen (BN) isosteric substitution has emerged as a powerful molecular design strategy that enables precise tuning of frontier orbital distributions and charge-transfer characteristics without disrupting the π-conjugated backbone.

Recent advances have shown that π-conjugated systems incorporating BN units can effectively modulate electronic polarization and intermolecular interactions, offering enhanced control over HOMO–LUMO alignment and optoelectronic response [17-20]. One of the most effective approaches in this regard is boron–nitrogen (BN) isosteric substitution [21]. The incorporation of BN units into aromatic systems preserves the overall conjugation while introducing localized polarity and altering the electronic distribution. This strategy enables fine control over HOMO–LUMO energy levels, charge separation characteristics, and molecular electrostatic potential, which are directly related to charge injection and recombination processes in OLED devices. From a structural perspective, naphthalimide-based acceptor units are particularly advantageous due to their strong electron affinity, rigid aromatic frameworks, and favorable photophysical properties. At the same time, carbazole derivatives contribute high hole-transport capability and chemical stability, making them ideal building blocks for bipolar OLED emitters [22, 23]. A recent experimental study has reported thermally stable and energy-efficient bipolar emitters based on naphthalimide–carbazole architectures, which are herein represented as compounds 1–3 [24]. As illustrated in Fig. 1, the representative molecular systems (1–3) exhibit distinct donor–π–acceptor architectures, where variations in the π-bridge and acceptor regions provide a structural basis for systematically exploring the electronic effects of BN incorporation. These materials exhibit high device performance and favorable optoelectronic properties, providing a reliable reference platform for evaluating structure–property relationships [19, 25-28]. However,

despite these experimental advances, the extent to which BN isosteric substitution can systematically modulate the electronic structure of such bipolar architectures remains to be fully elucidated, particularly with respect to position-dependent effects within the π-bridge and acceptor regions. Despite these promising experimental findings, a comprehensive theoretical interpretation that systematically correlates their electronic structure with the observed behavior remains limited. Consequently, a detailed computational investigation is required to bridge this gap and to provide a rational understanding of how BN doping influences donor–acceptor interactions and overall optoelectronic performance, thereby enabling more effective molecular design strategies for next-generation OLED emitters [29-31].

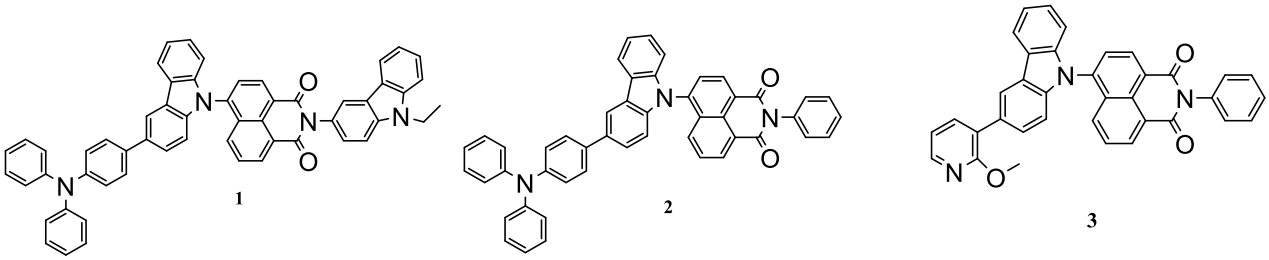

Fig. 1. Molecular structures of the reference naphthalimide–carbazole bipolar emitters (compounds 1–3) illustrating donor–π–acceptor architecture.

In this context, the present study aims to establish a robust and predictive structure–property–performance relationship for naphthalimide–carbazole-based bipolar OLED emitters by systematically investigating three representative molecular systems (1–3) that correspond to experimentally reported analogs. Although these systems have demonstrated promising optoelectronic performance, a comprehensive molecular-level understanding of how site-specific structural modifications influence electronic structure, charge-transfer characteristics, and device-relevant properties remains insufficiently resolved. To address this gap, a boron–nitrogen (BN) isosteric substitution strategy is selectively implemented across the donor, π-bridge, and acceptor regions to generate a series of position-dependent isomers while preserving the intrinsic donor–π–acceptor (D–π–A) framework. Density functional theory (DFT) and time-dependent DFT (TD-DFT) calculations are employed to systematically evaluate key electronic descriptors, including frontier molecular orbital energies, global reactivity parameters, molecular electrostatic potential (MEP) distributions, and excited-state transition characteristics. The results reveal that BN incorporation induces a pronounced spatial redistribution of frontier orbitals, enhances the intramolecular charge-transfer (ICT) character, and enables fine control of electronic polarization in a position-dependent manner. By directly correlating these theoretical insights with available experimental data for compounds 1–3, this study establishes a mechanistically grounded and experimentally consistent framework for rational molecular design, highlighting BN doping as an effective strategy to tune the electronic structure and optimize the performance of next-generation bipolar OLED emitters.

2. Computational Methods

All quantum chemical calculations were performed using Density Functional Theory (DFT) and Time-Dependent DFT (TD-DFT) as implemented in the Gaussian 16 software package (Revision C.01) [32]. Molecular structures were constructed and visualized using GaussView 6.0.8 [33]. The ground-state (S_0) geometries of all BN-doped position isomers were fully optimized at the B3LYP/6-311++G(d,p) level of theory without any symmetry constraints [34–36]. Excited-state calculations were carried out using TD-DFT at the B3LYP/6-31++G(d,p) level to evaluate the electronic excitation properties of the studied systems. This computational

protocol enables a reliable description of frontier molecular orbitals and related electronic transitions in π-conjugated donor–acceptor systems. Key electronic descriptors, including HOMO–LUMO energy levels, oscillator strengths, and transition dipole moments, were systematically analyzed to elucidate the effects of boron–nitrogen substitution on the electronic structure. In addition, molecular electrostatic potential (MEP) distributions were examined to provide insight into charge distribution and polarization characteristics. Overall, this computational framework enables consistent evaluation of structure–property relationships and provides a reliable theoretical basis for interpreting the influence of BN incorporation on the optoelectronic behavior of bipolar OLED emitters [37–41].

In addition to the electronic structure analysis, electrochemical descriptors were further computed to assess the charge-injection characteristics of the investigated systems. These parameters are directly related to the alignment of molecular energy levels at the electrode/organic interface, which critically influences the turn-on voltage and overall luminance efficiency of OLED devices. The following expressions were employed for their evaluation:

$$V_{onset-ox} = -E_{HOMO} - V_{ref} \quad [1]$$

$$V_{onset-red} = -E_{LUMO} - V_{ref} \quad [2]$$

$$E_{g-el} = E_{LUMO} - E_{HOMO} \quad [3]$$

$$E_{onset} = V_{onset-ox} + V_{onset-red}/2 \quad [4]$$

Four key electrochemical descriptors were evaluated to characterize charge injection and transport behavior in BN-doped position isomers. The onset oxidation potential ($V_{onset-ox}$)) corresponds to the energy required to remove an electron from the HOMO level and indicates hole-injection capability. In contrast, the onset reduction potential ($V_{onset-red}$)) reflects the energy associated with electron addition to the LUMO level and is directly related to electron injection efficiency. The electrochemical energy gap (E_{g-el})) represents the difference between LUMO and HOMO energies, providing insight into the intrinsic electronic structure and exciton formation characteristics of the molecule. The average onset potential (E_{onset}), defined as the mean of the oxidation and reduction onset values, serves as a practical descriptor of redox balance and charge neutrality in device environments. All electrochemical quantities were referenced to a constant electrode potential (V_{ref}) of 4.8 eV, corresponding to the standard ferrocene/ferrocenium (Fc/Fc^+) redox couple [42–46].

In this study, a set of quantum-chemical parameters and global reactivity descriptors were systematically computed to elucidate the structure–property relationships governing the optoelectronic performance of BN-doped positional isomers in OLED applications. These calculations provide detailed insight into the electronic factors controlling charge transport, exciton behavior, and emission efficiency, thereby establishing a link between molecular-level properties and device-relevant performance. The evaluated descriptors include HOMO and LUMO energy levels, the HOMO–LUMO energy gap (ΔE_{gap}), dipole moment, and conceptual DFT-based global reactivity indices such as chemical potential (μ), electronegativity (χ), chemical hardness (η), softness (σ), and electrophilicity (ω). These parameters play a central role in determining charge injection characteristics, electronic stability, and intermolecular interactions in OLED systems.Particular emphasis is placed on assessing how positional isomerism of boron–nitrogen units influences electronic distribution, charge-transfer characteristics, and overall optoelectronic behavior. In this context, global reactivity descriptors are employed to quantify the electron-

donating and electron-accepting tendencies of the molecules, providing mechanistic insight into their interaction potential within multilayer OLED architectures. A comprehensive analysis of μ, χ, η, and ω enables a predictive evaluation of molecular stability and reactivity under operational conditions, offering valuable guidelines for the rational design of efficient and stable OLED emitters [46–50].

$$\Delta Egap = E_{HOMO} - E_{LUMO} \quad [5]$$

$$IP = -E_{HOMO} \quad [6]$$

$$EA = -E_{LUMO} \quad [7]$$

$$\eta = \left(\frac{\mathrm{IP}-\mathrm{EA}}{2}\right) \quad [8]$$

$$\sigma = 1/\eta \quad [9]$$

$$\mu = -\chi = \left(\frac{IP+EA}{2}\right) \quad [10]$$

$$\omega^{-} = \frac{(3\mathrm{IP}+\mathrm{EA})^2}{(16(\mathrm{IP}-\mathrm{EA}))} \quad [11]$$

$$\omega^{+} = \frac{(\mathrm{IP}+3\mathrm{EA})^2}{(16(\mathrm{IP}-\mathrm{EA}))} \quad [12]$$

Following these definitions, a comprehensive evaluation of global reactivity descriptors including chemical hardness (η), softness (σ), electronegativity (χ), chemical potential (μ), and electrophilicity index (ω) was carried out to establish quantitative relationships between electronic structure, thermodynamic stability, and chemical reactivity. Since these descriptors are directly derived from frontier molecular orbital energies, they provide reliable insight into the intrinsic charge-transfer capability of BN-doped positional isomers, a key factor governing exciton dynamics and carrier balance in OLED systems. Additionally, the electroaccepting (ω^{+}) and electrodonating (ω^{-}) powers were calculated further to characterize the donor–acceptor nature of the molecules. This extended descriptor set enables a detailed reactivity mapping and offers mechanistic insight into intermolecular interactions within multilayer OLED architectures. All calculations were performed under standard conditions without empirical corrections, ensuring consistency and reproducibility of the obtained results.

3. Result and Discussion

Based on this systematic BN substitution strategy across the donor, π-bridge, and acceptor segments, the following section presents a detailed analysis of how position-dependent doping influences the electronic structure and charge-transfer characteristics of compounds 1–3. In this context, a comprehensive quantum-chemical analysis was performed to evaluate the optoelectronic suitability of BN-doped positional isomers for OLED applications. Key electronic properties, including frontier molecular orbital distributions, global reactivity descriptors, ionization potentials, electron affinities, and energy level alignments with interfacial layers, were systematically investigated. Particular emphasis was placed on elucidating how boron–nitrogen incorporation influences electronic distribution and donor–acceptor interactions. The obtained results provide detailed insight into the structure–property relationships governing charge transport and overall optoelectronic behavior in these systems.

3.1. Frontier Molecular Orbital Analysis of BN-Doped Position Isomers

The frontier molecular orbital (FMO) properties of compounds 1–3 and their BN-doped position isomers were systematically investigated to establish a comprehensive structure–property relationship governing electronic distribution, intramolecular charge transfer (ICT), and optoelectronic performance within naphthalimide–carbazole-based donor–π–acceptor (D–π–A) systems. As illustrated in Fig. 1, all optimized structures retain the intrinsic conjugated backbone upon BN incorporation, confirming that isosteric B–N substitution does not disrupt the overall molecular framework but instead introduces localized electronic perturbations that can be exploited for fine-tuning electronic properties [51-56].

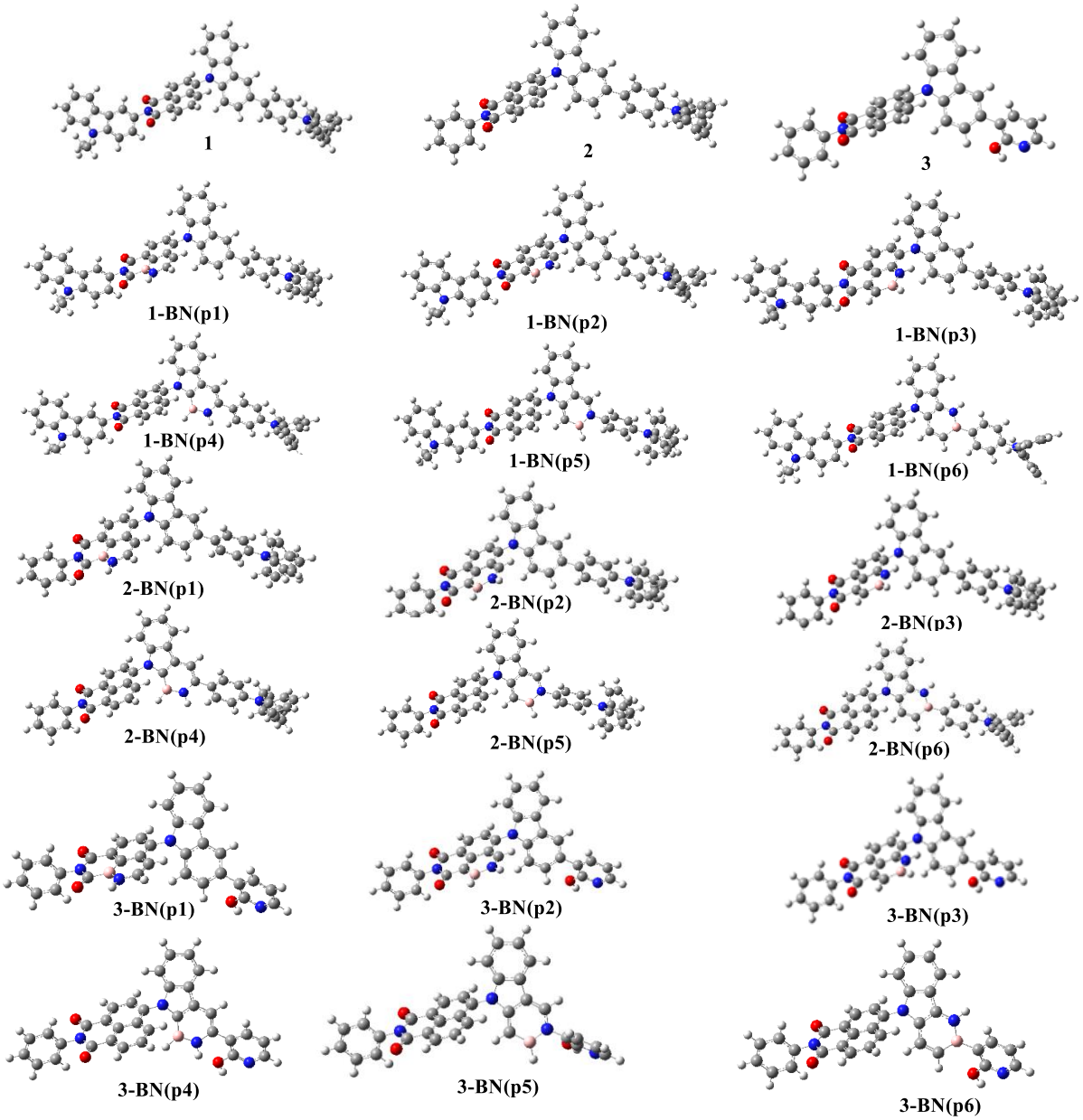

Fig. 1. Optimized structures of compounds 1–3 and their BN-doped position isomers.

Within this framework, the position-dependent nature of BN substitution plays a decisive role in modulating electronic behavior. Specifically, substitution at p1 primarily perturbs the donor (carbazole/triphenylamine) region, p2–p3 correspond to modifications along the π-bridge, and p4–p6 progressively approach the naphthalimide acceptor core. This spatial classification enables a direct interpretation of how BN doping influences orbital energies and charge-transfer pathways along the molecular backbone. A quantitative analysis of the computed energy levels presented in Table 1 reveals that the parent compounds exhibit HOMO energies of −5.226 eV (1), −5.248 eV (2), and −5.919 eV (3), with corresponding LUMO levels of −2.889 eV, −2.971 eV, and −2.981 eV. These values show good agreement with experimentally reported data (HOMO: −5.160, −5.050, −4.710 eV; LUMO: −2.760, −2.650, −2.470 eV) [24], thereby validating the computational methodology employed. Notably, compound 3 exhibits a significantly deeper HOMO level than experimental observations, indicating enhanced orbital stabilization and reduced donor–acceptor coupling, consistent with its more localized electronic structure.

Table 1. Electrochemical Parameters Derived from Frontier Molecular Orbital Energies of BN-Doped Position Isomers of Naphthalimide–Carbazole-Based Donor–π–Acceptor Systems

B-N Derivatives	HOMO eV	LUMO eV	$V_{onset\text{-}ox}$	$V_{onset\text{-}red}$	$E_{g\text{-}el}$	E_{onset}
	-5.226	**-2.889**	**0.426**	**-1.911**	**2.337**	**-0.743**
1	(-5.160)*	(-2.760)*				
1-BN(p1)	-5.202	-2.674	0.402	-2.126	2.528	-0.862
1-BN(p2)	-5.299	-3.038	0.499	-1.762	2.261	-0.631
1-BN(p3)	-5.262	-2.889	0.462	-1.911	2.373	-0.725
1-BN(p4)	-5.261	-2.723	0.461	-2.077	2.538	-0.808
1-BN(p5)	-5.412	-2.803	0.612	-1.997	2.609	-0.692
1-BN(p6)	-5.188	-2.886	0.388	-1.914	2.302	-0.763
	-5.248	**-2.971**	**0.443**	**-1.829**	**2.272**	**-0.693**
2	(-5.050)*	(-2.650)*				
2-BN(p1)	-5.222	-2.758	0.423	-2.042	2.464	-0.809
2-BN(p2)	-5.318	-3.106	0.518	-1.694	2.212	-0.588
2-BN(p3)	-5.282	-2.976	0.482	-1.824	2.306	-0.671
2-BN(p4)	-5.288	-2.801	0.488	-1.999	2.487	-0.756
2-BN(p5)	-5.433	-2.884	0.633	-1.916	2.549	-0.642
2-BN(p6)	-5.211	-2.967	0.411	-1.833	2.244	-0.711
	-5.919	**-2.981**	**1.119**	**-1.819**	**2.938**	**-0.350**
3	(-4.710)*	(-2.470)*				
3-BN(p1)	-5.843	-2.765	1.043	-2.035	3.078	-0.496
3-BN(p2)	-6.045	-3.121	1.245	-1.679	2.924	-0.218
3-BN(p3)	-6.028	-2.987	1.228	-1.813	3.041	-0.293
3-BN(p4)	-5.618	-2.823	0.818	-1.978	2.795	-0.579
3-BN(p5)	-5.748	-2.899	0.948	-1.901	2.850	-0.476
3-BN(p6)	-5.687	-2.982	0.887	-1.818	2.705	-0.466

*Values given in parentheses correspond to experimental HOMO and LUMO energy levels (Ref. [24]).

This behavior is further reflected in the calculated electrochemical band gaps ($E_{g\text{-}el}$), which follow the trend:

2 → 1 < 3 (2.272 < 2.337 << 2.938 eV).

The relatively smaller band gaps of compounds 1 and 2 indicate stronger electronic communication between the carbazole donor and the naphthalimide acceptor through the π-bridge. In contrast, the significantly larger band gap of compound 3 suggests reduced orbital overlap and increased localization. This trend is fully consistent with experimental observations, where compounds 1 and 2 exhibit superior optoelectronic performance compared to compound 3 [24].

The spatial distributions of frontier orbitals shown in Fig. 2–4 provide critical insight into these trends. The LUMO densities are consistently localized on the naphthalimide acceptor core across all derivatives, confirming that BN substitution preserves and even enhances the electron-accepting character of this unit. In contrast, the HOMO distributions show strong dependence on substitution position. For compounds 1 and 2, the HOMO is delocalized over the carbazole donor and partially extends into the π-bridge, indicating efficient π-conjugation and strong ICT character. However, a fundamentally different behavior is observed in Fig. 4 for compound 3, where HOMO densities become highly localized and fragmented, particularly in BN-doped derivatives. This pronounced fragmentation disrupts the continuity of π-conjugation, thereby significantly weakening donor–acceptor electronic coupling. As a consequence, the HOMO loses its extended delocalization across the molecular backbone. It becomes confined to isolated donor regions, resulting in diminished ICT efficiency and reduced charge transport capability compared to compounds 1 and 2. This explains why compound 3, despite having relatively stable energy levels, exhibits inferior optoelectronic performance.

The influence of BN substitution on charge injection processes is further elucidated through the onset potentials reported in Table 1. Compounds 1 and 2 exhibit relatively low oxidation onset potentials (0.426 V and 0.443 V), indicating favorable hole injection from the donor region. In contrast, compound 3 shows a significantly higher value (1.119 V), reflecting the energetic penalty associated with its deeper HOMO level. These variations in onset potentials directly influence charge-injection barriers at the electrode/organic interface, thereby affecting the device turn-on voltage and overall OLED efficiency. Similarly, the reduction onset potentials demonstrate that BN-induced lowering of LUMO energies, particularly for π-bridge substitutions (p2–p3), enhances electron injection capability by improving alignment with electron transport layers. The molecular electrostatic potential (MEP) surfaces presented in Fig. 2–4 further support these findings by revealing a pronounced increase in charge polarization upon BN incorporation. The electron-deficient regions remain centered on the naphthalimide acceptor, while electron-rich regions are localized on the carbazole donor; however, BN substitution amplifies this separation, particularly along the π-bridge. This enhanced polarization promotes directional charge transfer and facilitates exciton formation, which is essential for efficient OLED operation.

Overall, the combined analysis of Table 1 and Fig. 1–4 clearly demonstrates that BN doping exerts a strong position-dependent influence on both electronic structure and spatial orbital distribution. Substitution along the π-bridge enhances electron injection by lowering LUMO energies and improving orbital delocalization, whereas substitution near the acceptor stabilizes the electronic structure and increases orbital localization. Most importantly, the strong agreement between theoretical predictions and experimental observations confirms that BN-induced modulation of frontier orbitals directly governs device-relevant properties, establishing a robust and predictive framework for the rational design of advanced OLED materials. This study clearly demonstrates that BN doping provides a rational and highly effective strategy for fine-tuning both electronic structure and device-relevant properties, offering direct design guidelines for next-generation high-efficiency OLED emitters.

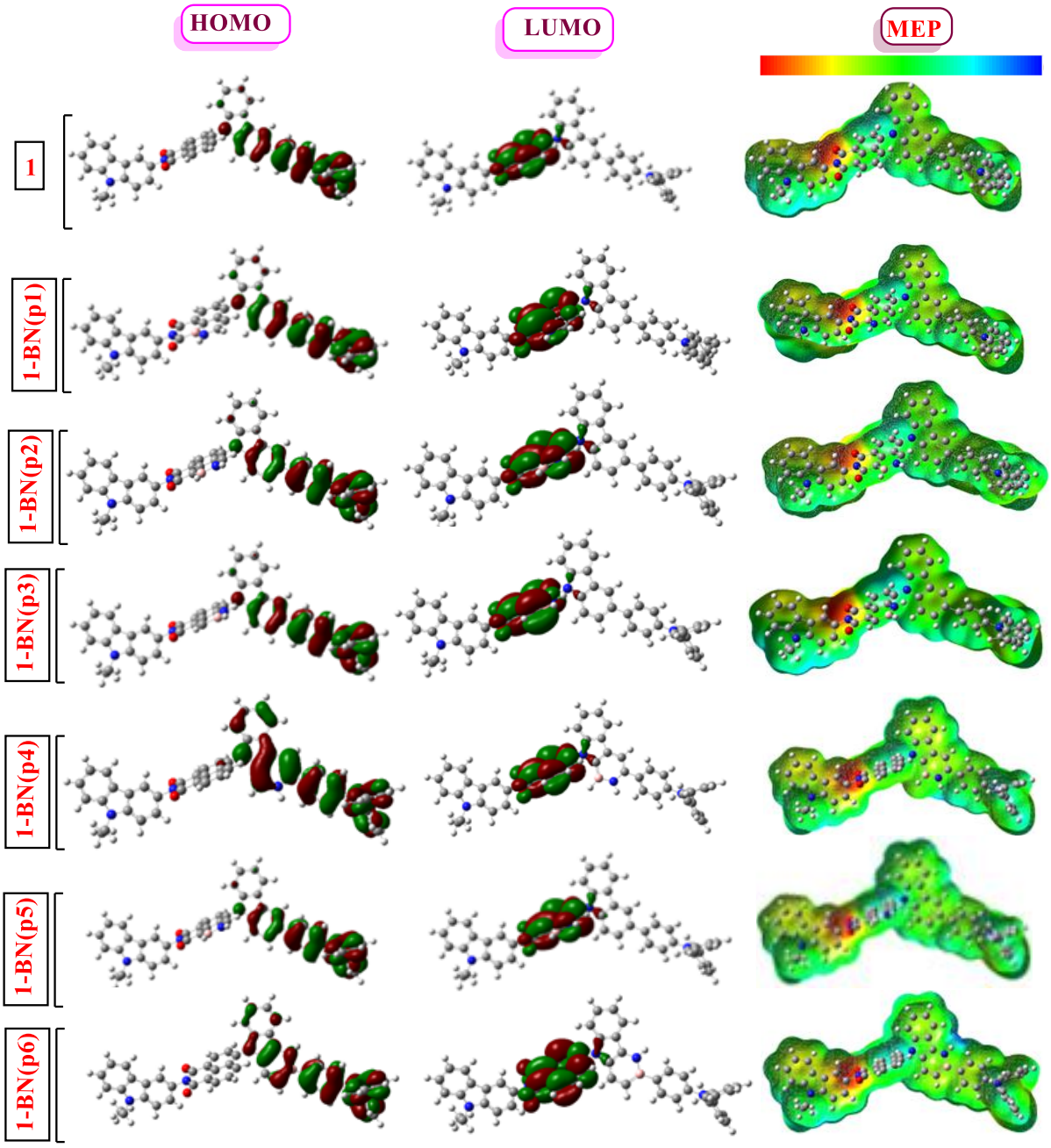

Fig. 2. HOMO, LUMO, and MEP distributions of compound 1 and its BN-doped position isomers.

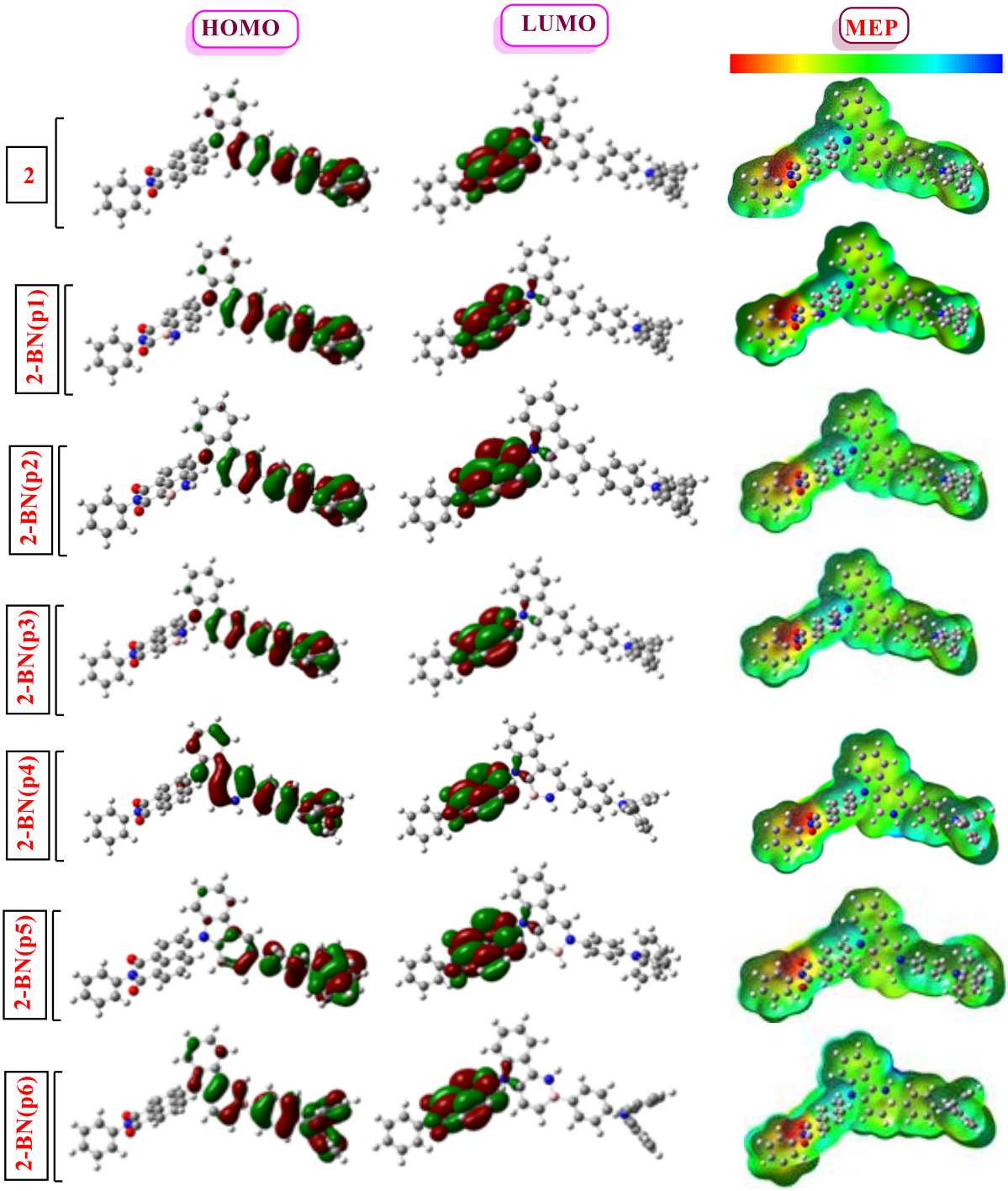

Fig. 3. HOMO, LUMO, and MEP distributions of compound 2 and its BN-doped position isomers.

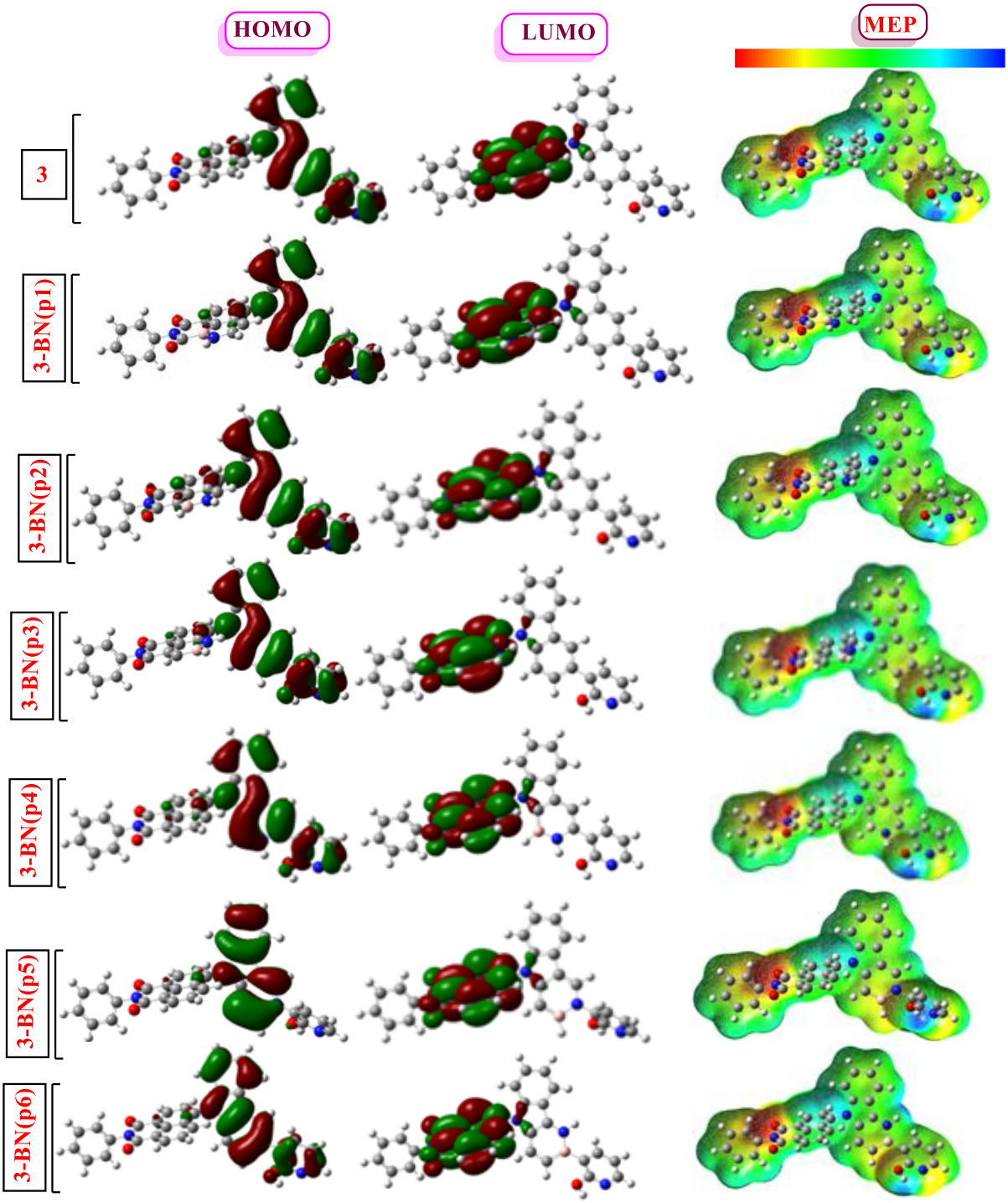

Fig. 4. HOMO, LUMO, and MEP distributions of compound 3 and its BN-doped position isomers.

Building upon these insights, a more nuanced picture emerges when the interplay between orbital topology and position-specific BN incorporation is considered in terms of charge-transport anisotropy along the molecular backbone. In particular, derivatives featuring BN substitution within the π-bridge region (p2–p3) exhibit a more continuous electronic pathway between the carbazole donor and the naphthalimide acceptor, as evidenced by the smoother phase progression of frontier orbitals and the reduced energetic separation between charge injection levels. This continuity facilitates not only enhanced electron mobility but also a more balanced charge recombination profile within the emissive layer. In contrast, substitution patterns approaching the acceptor core

(p4–p6) introduce localized electrostatic perturbations that, while stabilizing the LUMO, partially disrupt the coherence of the π-system, leading to anisotropic charge transport and reduced overlap between frontier orbitals. This distinction becomes particularly critical under device-relevant conditions, where subtle differences in orbital connectivity can dictate exciton formation zones and recombination efficiency. Consequently, the ability to selectively position BN units along the π-bridge provides a strategic handle for engineering charge flow pathways at the molecular level, enabling simultaneous optimization of carrier balance and emission characteristics without altering the fundamental D–π–A scaffold.

3.2. Global Reactivity Descriptors and Electronic Structure Modulation in BN-Doped Donor–π–Acceptor Systems

To further substantiate the structure–property relationships established in Section 3.1 through frontier orbital distributions and electrochemical parameters, a detailed evaluation of global reactivity descriptors (GRDs) was performed. These descriptors, summarized in Table 2, provide a quantitative framework for interpreting molecular electronic responsiveness, charge stabilization capability, and redox adaptability in BN-doped naphthalimide–carbazole-based donor–π–acceptor systems. The calculated parameters, including ionization potential (IP), electron affinity (EA), chemical hardness (η), softness (σ), electronegativity (χ), chemical potential (μ), electrophilicity index (ω), and electroaccepting/electrodonating powers (ω^+/ω^-), collectively describe the intrinsic tendency of a molecule to participate in charge transfer processes. Unlike conventional analyses based solely on HOMO–LUMO gaps, these descriptors provide deeper mechanistic insight into how BN substitution modulates electronic flexibility and charge-accommodation capacity, both of which are essential for OLED performance [57-59].

Table 2. Computed Global Reactivity Descriptors and Ionization Parameters of BN-Doped Position Isomers in Naphthalimide–Carbazole-Based Donor–π–Acceptor Systems

B-N Derivatives	GRPs*										
	IP	**EA**	**E_{gap}**	**η**	**σ**	**χ**	**μ**	**ω**	**ε**	**ω+**	**ω-**
1	**5.226**	**2.889**	**2.337**	**1.169**	**0.856**	**4.058**	**-4.058**	**7.045**	**0.142**	**5.161**	**9.219**
1-BN(p1)	5.202	2.674	2.528	1.264	0.791	3.938	-3.938	6.134	0.163	4.323	8.262
1-BN(p2)	5.299	3.038	2.261	1.131	0.885	4.169	-4.169	7.686	0.130	5.743	9.912
1-BN(p3)	5.262	2.889	2.373	1.186	0.843	4.075	-4.075	7.000	0.143	5.111	9.186
1-BN(p4)	5.261	2.723	2.538	1.269	0.788	3.992	-3.992	6.279	0.159	4.442	8.434
1-BN(p5)	5.412	2.803	2.609	1.304	0.767	4.108	-4.108	6.468	0.155	4.577	8.685
1-BN(p6)	5.188	2.886	2.302	1.151	0.869	4.037	-4.037	7.081	0.141	5.206	9.244
2	**5.248**	**2.971**	**2.277**	**1.138**	**0.879**	**4.109**	**-4.109**	**7.418**	**0.135**	**5.506**	**9.615**
2-BN(p1)	5.223	2.758	2.464	1.232	0.812	3.991	-3.991	6.462	0.155	4.621	8.612
2-BN(p2)	5.318	3.106	2.212	1.106	0.904	4.212	-4.212	8.018	0.125	6.051	10.263
2-BN(p3)	5.282	2.976	2.306	1.153	0.867	4.129	-4.129	7.395	0.135	5.475	9.604
2-BN(p4)	5.288	2.801	2.487	1.243	0.804	4.044	-4.044	6.577	0.152	4.710	8.755
2-BN(p5)	5.433	2.884	2.549	1.274	0.785	4.158	-4.158	6.784	0.147	4.864	9.022
2-BN(p6)	5.211	2.967	2.244	1.122	0.891	4.089	-4.089	7.452	0.134	5.548	9.637
3	**5.919**	**2.981**	**2.938**	**1.469**	**0.681**	**4.450**	**-4.450**	**6.741**	**0.148**	**4.700**	**9.150**
3-BN(p1)	5.843	2.765	3.078	1.539	0.650	4.304	-4.304	6.019	0.166	4.059	8.364
3-BN(p2)	6.045	3.121	2.924	1.462	0.684	4.583	-4.583	7.184	0.139	5.075	9.658
3-BN(p3)	6.028	2.987	3.041	1.520	0.658	4.507	-4.507	6.682	0.150	4.618	9.125
3-BN(p4)	5.618	2.823	2.796	1.398	0.715	4.221	-4.221	6.372	0.157	4.437	8.658
3-BN(p5)	5.748	2.899	2.850	1.425	0.702	4.324	-4.324	6.560	0.152	4.577	8.900
3-BN(p6)	5.687	2.982	2.705	1.352	0.739	4.334	-4.334	6.946	0.144	4.948	9.283

*The values for σ and ε are given in eV^{-1}, while all other GRD values are presented in eV.

Consistent with the trends observed in Table 1, the parent compounds exhibit a clear differentiation in reactivity profiles. Compound 3 shows relatively higher chemical hardness (η = 1.469 eV) and lower softness (σ = 0.681 eV^{-1}), indicating a more rigid electronic structure with reduced adaptability toward charge transfer. In contrast, compounds 1 and 2 display lower hardness values (η = 1.169 and 1.138 eV), suggesting enhanced polarizability and greater responsiveness to electronic perturbation. These findings are fully consistent with the HOMO–LUMO delocalization patterns discussed in Section 3.1, where compounds 1 and 2 exhibited stronger donor–π–acceptor coupling and more efficient ICT behavior. A more detailed analysis of BN-doped derivatives reveals a strong position-dependent modulation of GRDs across the p1–p6 substitution sites. In particular, π-bridge substitutions (p2–p3) consistently yield lower hardness and higher softness, indicating improved electronic flexibility and enhanced charge-transfer capability. For example, 2-BN(p2) (η = 1.106 eV; σ = 0.904 eV^{-1}) and 3-BN(p2) (η = 1.462 eV; σ = 0.684 eV^{-1}) demonstrate optimized reactivity profiles, which correlate directly with the improved LUMO stabilization and electron injection behavior identified in Section 3.1. Similarly, electrophilicity index (ω) and electroaccepting power (ω^+) provide critical insight into the ability of these systems to accommodate incoming electrons. Derivatives such as 2-BN(p3) and 2-BN(p6), with relatively high ω values (~4.13–4.09) and elevated ω^+ values (>5.4 eV), indicate strong electron-accepting capability, which is essential for efficient electron transport in OLED devices. This observation aligns directly with the previously discussed LUMO localization on the naphthalimide acceptor core, confirming that BN substitution enhances the system's intrinsic electron affinity without altering its fundamental electronic topology.

In contrast, substitutions closer to the acceptor region (p4–p5) tend to increase chemical hardness and reduce electrophilicity, as observed for 1-BN(p4) (η = 1.269 eV; ω = 3.992) and 2-BN(p5) (η = 1.274 eV; ω = 4.158). This behavior reflects increased orbital localization and reduced electronic communication within the π-system, consistent with the partially confined HOMO distributions observed in Fig. 2 and Fig. 3. Such localization effects reduce charge-transfer efficiency and may lead to less balanced carrier transport under device conditions. A particularly important observation emerges when comparing derivatives of compound 3 with compounds 1 and 2. Despite exhibiting relatively high electrophilicity values in certain cases (e.g., 3-BN(p3), ω = 4.507), the overall reactivity of compound 3 remains limited due to its consistently higher hardness and lower softness values. This confirms that electrophilicity alone is insufficient to ensure efficient charge transport; rather, an optimal balance between hardness, softness, and charge distribution is required. This finding directly supports the HOMO fragmentation behavior observed in Fig. 4, where reduced orbital delocalization leads to diminished electronic coupling and poorer charge-transport performance. The chemical potential (μ) and electronegativity (χ) values further reinforce these trends, as they remain relatively symmetric (μ = −χ) across all systems, indicating stable electronic configurations. However, subtle variations in these parameters—particularly in π-bridge-substituted derivatives — suggest improved charge balance, which is critical for minimizing recombination losses in OLED devices.

Importantly, the consistency between GRDs in Table 2, orbital distributions in Fig. 2–4, and electrochemical parameters in Table 1 demonstrates the robustness of the applied computational approach. The observed correlation confirms that BN-induced electronic modulation is not only reflected in frontier orbital energies but also quantitatively captured by scalar reactivity descriptors. Furthermore, the trends observed in GRDs

are in strong agreement with experimentally reported optoelectronic performance, with materials exhibiting lower hardness, higher electrophilicity, and balanced charge-injection characteristics demonstrating superior OLED efficiency. This agreement highlights the predictive capability of GRDs as reliable descriptors for screening high-performance emissive materials.

Overall, this analysis establishes that BN substitution serves as a powerful, position-sensitive tuning mechanism, in which π-bridge modifications enhance electronic flexibility and charge transfer. In contrast, acceptor-proximal substitutions increase stability at the expense of reactivity. These findings provide a mechanistically grounded framework linking molecular topology to electronic function, demonstrating that precise dopant placement enables targeted optimization of both reactivity and optoelectronic performance.

3.3. Position-Dependent Energy Level Alignment and Charge Injection in BN-Doped Donor–π–Acceptor Systems

The meticulous alignment of energy levels across emissive, transport, and interfacial layers critically governs the performance of OLED devices. Building upon the electronic structure insights obtained in Sections 3.1 and 3.2, the energy level alignment of compounds 1–3 and their BN-doped position isomers was systematically evaluated with respect to representative HTL and ETL materials, as illustrated in Fig. 5. Since the pioneering multilayer OLED architecture proposed by Tang and VanSlyke, the integration of charge transport and emissive layers has been recognized as a key strategy for optimizing charge injection and recombination processes [60, 61]. For efficient hole injection, the HOMO level of the emissive layer must be lower than that of the HTL (HOMO_HTL > HOMO_EML), ensuring a thermodynamically favorable downhill transition [62,63]. As shown in Fig. 5, compounds 1 and 2 and their BN-doped derivatives (particularly p2–p5) exhibit HOMO levels in the range of approximately −5.0 to −5.6 eV, which align well with commonly used HTLs such as PEDOT:PSS (~−5.0 eV), Spiro-TPD (~−5.3 eV), and TFB (~−5.4 eV). This favorable energy alignment minimizes hole-injection barriers and facilitates efficient carrier transfer across the HTL/EML interface, resulting in reduced turn-on voltage and enhanced hole-injection efficiency, in accordance with established OLED design principles [64–66].

In contrast, compound 3 exhibits a significantly deeper HOMO level (~−5.9 eV), resulting in a larger injection barrier relative to these HTLs, which is expected to increase the turn-on voltage and reduce hole-injection efficiency in device operation. This behavior directly correlates with the HOMO localization and fragmentation observed in Fig. 4, and with the higher chemical hardness identified in Section 3.2, both of which indicate reduced electronic coupling and inferior hole-transport characteristics. Importantly, experimental findings support this trend: materials with HOMO levels ranging from −5.16 to −5.05 eV exhibit lower driving voltages and higher efficiency, whereas deeper HOMO levels lead to increased injection barriers and reduced device performance. This provides direct validation of the superior hole-injection characteristics predicted for compounds 1 and 2 relative to compound 3. Electron injection is subject to the complementary requirement that LUMO_EML < LUMO_ETL. As illustrated in Fig. 5, the LUMO levels of the BN-doped derivatives (~−2.7 to −3.1 eV) form favorable energy offsets with widely used ETL materials such as PEIE, Liq, TPN2, ZnO, and TiO_2, whose LUMO levels lie between −1.5 and −2.0 eV [67,68]. This alignment establishes a thermodynamically favorable pathway for electron injection with a small energy barrier, facilitating efficient charge transfer from the cathode into the emissive layer. A clear position-dependent trend emerges when comparing BN substitution sites. π-bridge substitutions (p2–p3) lead to more-stabilized LUMO levels and improved alignment with ETLs, thereby enhancing electron injection

efficiency. This observation is fully consistent with Section 3.2, where these derivatives exhibited higher electrophilicity (ω) and electroaccepting power (ω^+), confirming their enhanced ability to accommodate incoming electrons. In contrast, substitutions near the acceptor region (p5–p6) increase orbital localization, slightly reducing alignment efficiency.

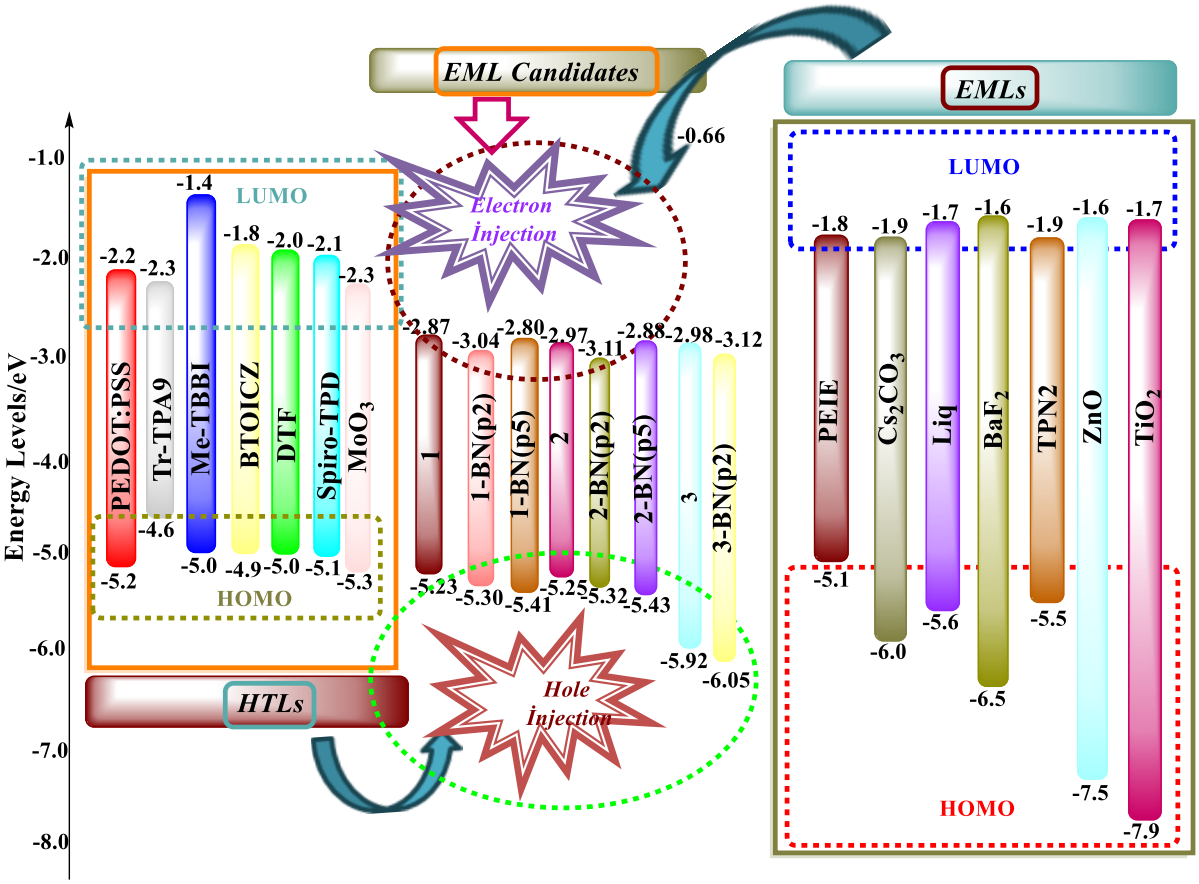

Fig. 5. Figure 3. Energy-level alignment diagram of compounds 1–3 and selected BN-doped positional isomers relative to representative HTL and ETL materials, illustrating position-dependent modulation of charge-injection characteristics.

The combined HOMO–LUMO alignment reveals that compounds 1 and 2, and their π-bridge-substituted derivatives, exhibit a more balanced charge-injection profile than compound 3. This balance is essential for efficient exciton formation and recombination within the emissive layer, as it minimizes charge accumulation and reduces non-radiative losses. Furthermore, the bidirectional charge injection pathways illustrated in Fig. 5 highlight the ambipolar character of selected BN-doped derivatives, particularly those substituted at intermediate positions (p2–p4). These systems simultaneously satisfy both hole and electron injection criteria, enabling efficient carrier transport across the device. This behavior directly correlates with the GRD trends discussed in Section 3.2, in which lower hardness and higher softness values indicate enhanced electronic adaptability. From a device-oriented perspective, this alignment directly impacts key performance parameters such as turn-on voltage, luminance efficiency, and charge balance. Materials with HOMO and LUMO levels well-matched to those of the HTL and ETL layers exhibit reduced injection barriers and improved recombination efficiency. In contrast, systems

with deeper HOMO levels and localized orbitals, such as compound 3, require higher operating voltages and exhibit poorer charge-transport characteristics.

Overall, the energy level alignment analysis presented in Fig. 5, together with the orbital topology (Section 3.1) and GRD analysis (Section 3.2), establishes a coherent structure–property–device relationship. BN doping emerges as a rational and highly effective molecular design strategy, enabling precise position-dependent control over interfacial energetics and charge-injection characteristics, while π-bridge modifications further enhance charge injection and transport efficiency. At the same time, donor- and acceptor-proximal substitutions modulate orbital localization and stability. This integrated framework provides a rational basis for designing high-performance OLED emitters with optimized charge injection and transport characteristics.

3.6. Excited-State Properties of BN-Doped Position Isomers

The excited-state properties of compounds 1–3 and their BN-doped positional isomers were systematically analyzed to establish a direct correlation among electronic-structure modulation, optical transitions, and device-relevant optoelectronic behavior. In particular, the simulated UV–Vis absorption spectra provide critical insight into excitation characteristics and intramolecular charge transfer (ICT), which are closely linked to OLED performance and thermally activated delayed fluorescence (TADF) mechanisms, where BN incorporation plays a key role in tuning singlet–triplet energy splitting and emission efficiency [19, 69, 70]. The simulated UV–Vis absorption spectra, presented in Fig. 6–8, provide critical insight into the nature of electronic excitations, oscillator strength distribution, and intramolecular charge transfer (ICT) characteristics, thereby complementing the frontier orbital (Section 3.1), GRD (Section 3.2), and energy level alignment (Section 3.3) analyses. A consistent spectral feature across all systems is the presence of two distinct absorption regimes: (i) a high-intensity band in the ~280–320 nm region and (ii) a lower-intensity, red-shifted band extending into the ~340–420 nm region. The former is primarily associated with localized π–π* transitions within the conjugated framework. At the same time, the latter corresponds to ICT transitions involving charge transfer from the carbazole-based donor to the naphthalimide acceptor core. This assignment is fully consistent with the HOMO–LUMO spatial separation discussed in Section 3.1, where HOMO densities are predominantly localized on the donor segments, and LUMO densities are strongly confined to the naphthalimide acceptor.

For compound 1 (Fig. 6), the dominant absorption band is centered around ~300 nm, exhibiting high oscillator strength, indicative of strongly allowed π–π* transitions arising from extensive conjugation across the donor–π–acceptor backbone. Upon BN substitution, a pronounced position-dependent modulation of spectral features is observed. In particular, π-bridge substitutions (p2–p3) induce noticeable bathochromic shifts in the ICT region, accompanied by the emergence of broader and more intense low-energy absorption tails. This behavior reflects enhanced donor–acceptor electronic coupling and improved orbital overlap, consistent with the increased softness and electrophilicity identified in Section 3.2. In contrast, substitutions near the acceptor (p5–p6) lead to slight hypsochromic shifts and reduced intensity in the ICT band, indicating increased orbital localization and diminished charge-transfer efficiency. A similar trend is observed for compound 2 (Fig. 7), although the spectral response is more pronounced due to its inherently stronger donor–acceptor interaction. The main absorption peak (~300 nm) remains dominant; however, BN substitution at the π-bridge (particularly at p2) significantly enhances the low-energy absorption band (~350–400 nm), accompanied by increased oscillator strength. This indicates a stronger ICT character and improved electronic delocalization, which directly correlates with the lower chemical

hardness and higher electron-accepting power reported in Table 2. Notably, the red-shifted absorption observed for these derivatives suggests a reduced excitation energy, which is highly favorable for OLED applications as it enables more efficient exciton generation and lower energy loss during charge recombination.

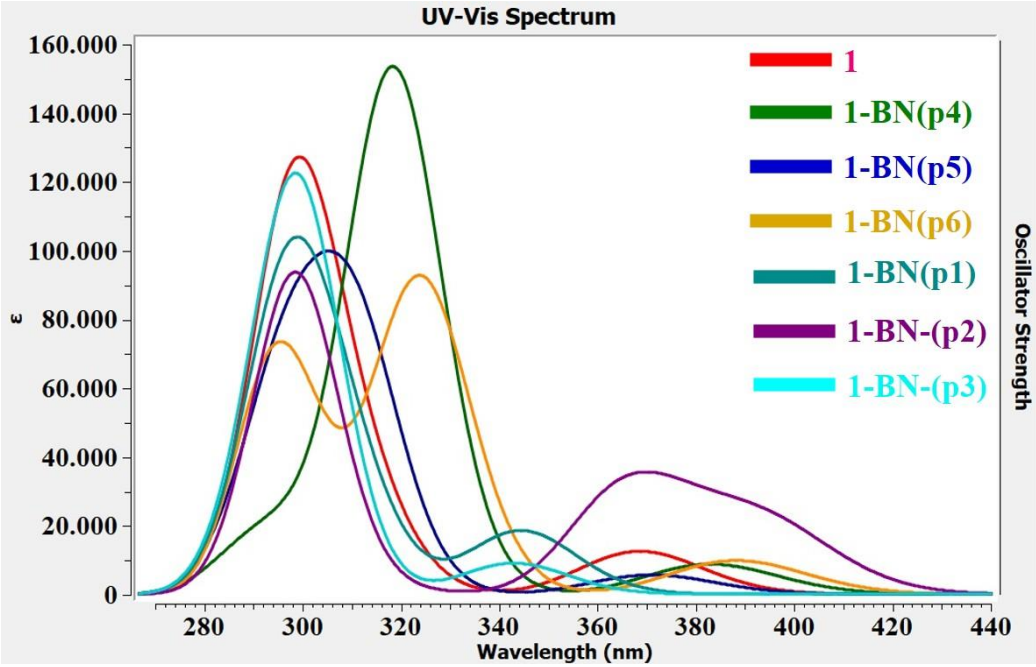

Fig. 6. Simulated UV–Vis spectra of compound 1 and its BN-doped position isomers

In contrast, compound 3 (Fig. 8) exhibits a fundamentally different excited-state behavior. The dominant absorption band is blue-shifted (~260–280 nm) and significantly narrower, indicating a more localized π–π* transition with reduced conjugation length. This observation is fully consistent with the HOMO fragmentation and increased orbital localization identified in Section 3.1. Although BN substitution still induces position-dependent variations, the extent of spectral modulation is comparatively limited. Even in π-bridge substituted derivatives (p2–p3), the ICT band remains weak and less pronounced, confirming that electronic communication between donor and acceptor units is inherently restricted in this system. This is further supported by the higher chemical hardness and reduced softness values reported in Table 2, which indicate limited electronic flexibility. A particularly important observation emerges when comparing oscillator strength distributions across the three systems. Compounds 1 and 2 exhibit strong oscillator strengths in both the π–π* and ICT regions, indicating efficient electronic transitions and strong light-absorbing capability. In contrast, compound 3 displays significantly weaker oscillator strengths in the ICT region, reflecting reduced transition probability and less efficient charge-transfer excitation. This directly affects radiative recombination efficiency and is expected to lead to inferior OLED performance.

Importantly, these theoretical predictions are in strong agreement with experimental observations, where materials exhibiting red-shifted absorption and enhanced ICT character demonstrate improved electroluminescent efficiency and lower energy losses. In particular, compounds with stronger donor–acceptor coupling and broader

absorption profiles are reported to show higher luminance efficiency and more balanced charge transport, directly validating the trends observed for compounds 1 and 2 relative to compound 3.

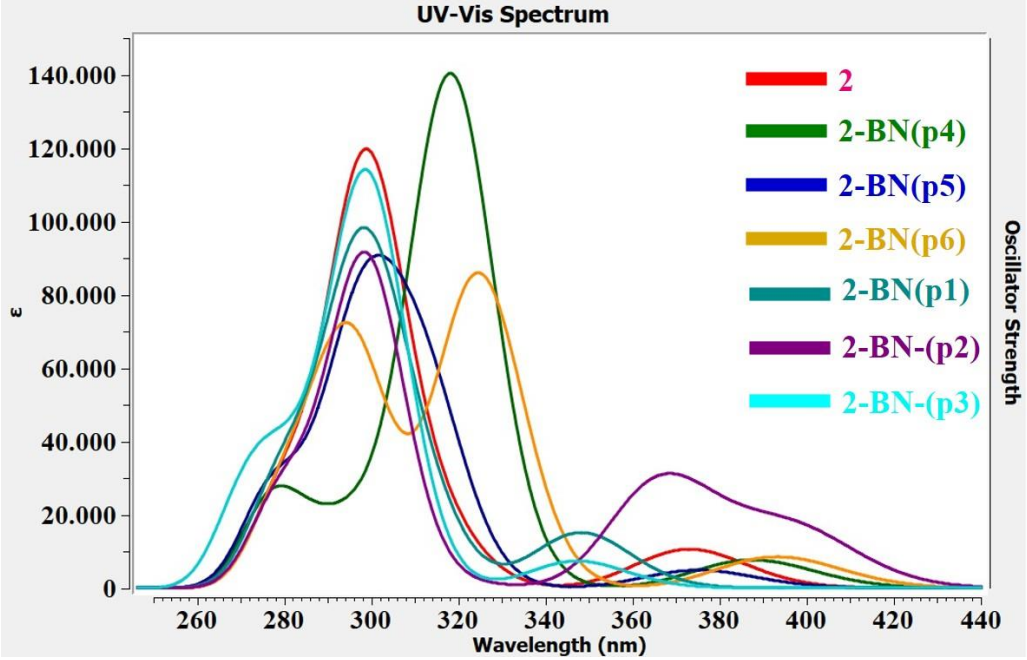

Fig. 7. Simulated UV–Vis spectra of compound 2 and its BN-doped position isomers

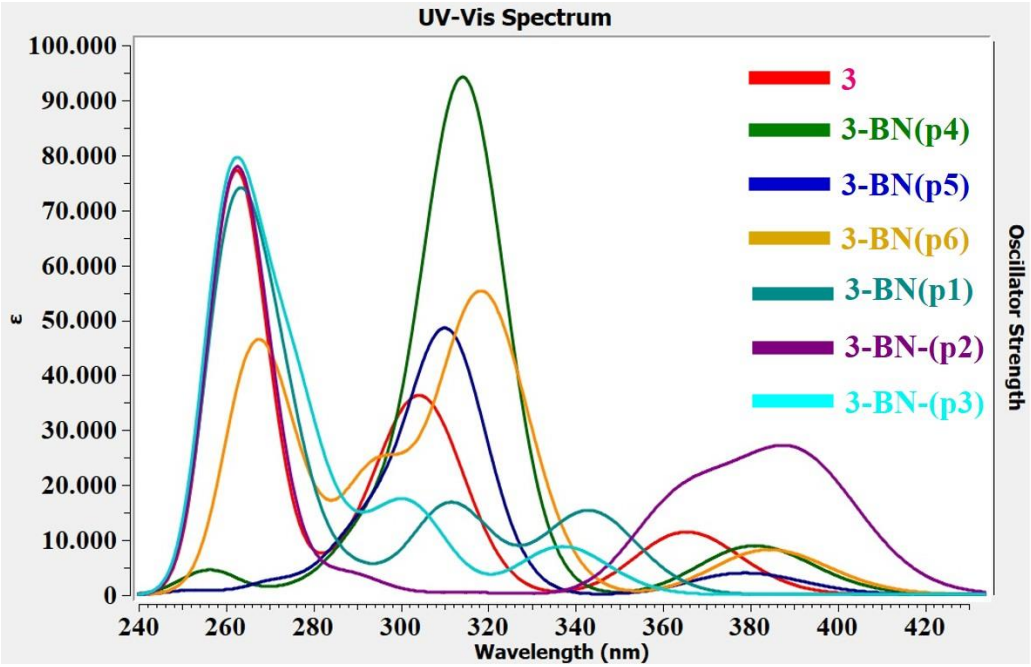

Fig. 8. Simulated UV–Vis spectra of compound 3 and its BN-doped position isomers

The position-dependent effect of BN doping provides further mechanistic insight. Substitution along the π-bridge (p2–p3) enhances conjugation continuity and facilitates charge delocalization, resulting in red-shifted absorption and increased oscillator strength. Conversely, substitutions near the acceptor (p5–p6) introduce localized electronic perturbations that partially disrupt conjugation, thereby reducing ICT intensity. Donor-proximal substitutions (p1) exhibit intermediate behavior, indicating partial modulation of electronic structure

without significantly altering the overall transition character. Collectively, the excited-state analysis presented in Figs. 6–8 establishes a clear and consistent relationship between molecular structure, electronic distribution, and optical response. The results demonstrate that BN doping is a highly effective, position-sensitive strategy for tuning excited-state properties, in which π-bridge modifications maximize ICT efficiency and optical absorption. At the same time, acceptor- and donor-proximal substitutions provide finer control over spectral characteristics. This comprehensive analysis, when combined with the orbital topology (Section 3.1), GRD trends (Section 3.2), and energy level alignment (Section 3.3), provides a unified framework for understanding and optimizing the optoelectronic behavior of BN-doped naphthalimide–carbazole systems. Importantly, it highlights that precise control over substitution position enables simultaneous tuning of electronic structure, charge transfer, and optical transitions, thereby offering a rational pathway for the design of next-generation high-performance OLED emitters.

4. Conclusion

This study provides a comprehensive and mechanistically consistent understanding of how BN isosteric substitution governs the electronic structure, charge-transfer behavior, and optoelectronic performance of naphthalimide–carbazole-based bipolar OLED emitters. By integrating frontier molecular orbital analysis, global reactivity descriptors, energy level alignment, and excited-state properties, a clear and unified structure–property–device relationship has been established. The results demonstrate that the intrinsic performance differences among compounds 1–3 arise from their distinct donor–π–acceptor coupling strengths, with compounds 1 and 2 exhibiting superior electronic delocalization, stronger intramolecular charge transfer (ICT), and more favorable charge-injection characteristics than compound 3. This theoretical prediction is in strong agreement with experimental observations, confirming the reliability of the computational framework used. Most importantly, BN doping emerges as a highly effective, position-sensitive strategy for fine-tuning molecular properties without disrupting the π-conjugated backbone. Substitution along the π-bridge (p2–p3) significantly enhances orbital delocalization, reduces chemical hardness, stabilizes the LUMO levels, and strengthens ICT transitions, thereby improving charge-injection balance and optical response. In contrast, substitutions near the acceptor region (p5–p6) increase orbital localization and electronic stability but partially suppress charge-transfer efficiency, while donor-proximal substitutions (p1) provide intermediate modulation.

The excited-state analysis further confirms that BN incorporation enables controlled tuning of optical transitions, with π-bridge substitutions inducing bathochromic shifts and enhancing oscillator strength, thereby improving light absorption and exciton formation efficiency. These effects, combined with optimized energy level alignment, highlight the critical role of BN doping in reducing injection barriers and enabling balanced charge transport under device conditions.

Overall, this study clearly demonstrates that BN doping offers a rational and highly effective molecular engineering strategy to simultaneously control the electronic structure, charge-transfer dynamics, and optoelectronic response. The strong agreement between theoretical predictions and experimental data underscores the predictive power of the adopted approach and establishes a reliable design principle for next-generation OLED materials. By revealing the decisive role of the substitution position in governing both ground- and excited-state properties, this work offers a practical and scalable pathway for the targeted design of high-efficiency bipolar emitters, thereby advancing OLED technology toward improved performance, stability, and energy efficiency.

Acknowledgments

We want to express our sincere gratitude to TÜBİTAK ULAKBİM and the High Performance and Grid Computing Center (TR-Grid e-Infrastructure) for granting us access to advanced computational facilities and for their ongoing technical support during this study. The high-performance computing resources and expert guidance provided by TR-Grid have been crucial in enabling complex quantum-chemical simulations and successfully achieving our research objectives.

Author contributions

Nihat Karakuş: Supervision, Project administration, Data collection, Formal analysis, Conceptualization, Writing - Review & Editing

Goncagül Serdaroğlu: Data collection, Formal analysis, Conceptualization, Writing - Review & Editing

All authors read and approved the final manuscript.

Funding Declaration

No funding.

Data availability

Data will be made available on request.

Declarations

Ethical approval

Not applicable.

Competing interests

The authors declare no competing interests

References

[1] Tang, C. W., & VanSlyke, S. A. (1987). Organic electroluminescent diodes. Applied physics letters, 51(12), 913-915.

[2] Baldo, M. A., O'Brien, D. F., You, Y., Shoustikov, A., Sibley, S., Thompson, M. E., & Forrest, S. R. (2023). Highly efficient phosphorescent emission from organic electroluminescent devices. In Electrophosphorescent Materials and Devices (pp. 1-11). Jenny Stanford Publishing.

[3] Reineke, S., Lindner, F., Schwartz, G., Seidler, N., Walzer, K., Lüssem, B., & Leo, K. (2009). White organic light-emitting diodes with fluorescent tube efficiency. Nature, 459(7244), 234-238.

[4] Coropceanu, V., Cornil, J., da Silva Filho, D. A., Olivier, Y., Silbey, R., & Brédas, J. L. (2007). Charge transport in organic semiconductors. Chemical reviews, 107(4), 926-952.

[5] Beresneviciute, R., Gautam, P., Nagar, M. R., Krucaite, G., Tavgeniene, D., Jou, J. H., & Grigalevicius, S. (2023). Naphtalimide-Based Bipolar Derivatives Enabling High-Efficiency OLEDs. Molecules, 28(16), 6027.

[6] Tang, G., Yang, W., & Zhao, J. (2022). Naphthalimide–carbazole compact electron donor–acceptor dyads: Effect of molecular geometry and electron-donating capacity on the spin-orbit charge transfer intersystem crossing. The Journal of Physical Chemistry A, 126(23), 3653-3668.

[7] Nagar, M. R., Kumar, K., Blazevicius, D., Beresneviciute, R., Krucaite, G., Tavgeniene, D., & Grigalevicius, S. (2023). Solution processable carbazole-benzophenone derivatives as bipolar hosts enabling high-efficiency stable green TADF organic LEDs. Journal of Materials Chemistry C, 11(4), 1579-1592.

[8] Dong, Q., Tai, F., Lian, H., Chen, Z., Hu, M., Huang, J., & Wong, W. Y. (2017). Thermally stable bipolar host materials for high efficiency phosphorescent green and blue organic light-emitting diodes. Dyes and Pigments, 143, 470-478.

[9] Hussain, M., El-Zohry, A. M., Hou, Y., Toffoletti, A., Zhao, J., Barbon, A., & Mohammed, O. F. (2021). Spin–orbit charge-transfer intersystem crossing of compact naphthalenediimide-carbazole electron-donor–acceptor triads. The Journal of Physical Chemistry B, 125(38), 10813-10831.

[10] Gudeika, D., Grazulevicius, J. V., Sini, G., Bucinskas, A., Jankauskas, V., Miasojedovas, A., & Jursenas, S. (2014). New derivatives of triphenylamine and naphthalimide as ambipolar organic semiconductors: experimental and theoretical approach. Dyes and Pigments, 106, 58-70.

[11] Ledwon, P. (2019). Recent advances of donor-acceptor type carbazole-based molecules for light emitting applications. Organic Electronics, 75, 105422.

[12] Siddiqui, I., Gautam, P., Blazevicius, D., Jayakumar, J., Lenka, S., Tavgeniene, D., & Jou, J. H. (2024). Bicarbazole-benzophenone based twisted donor-acceptor derivatives as potential blue TADF emitters for OLEDs. Molecules, 29(7), 1672.

[13] Tang, G., Yang, W., & Zhao, J. (2022). Naphthalimide–carbazole compact electron donor–acceptor dyads: Effect of molecular geometry and electron-donating capacity on the spin-orbit charge transfer intersystem crossing. The Journal of Physical Chemistry A, 126(23), 3653-3668.

[14] Brédas, J. L., Beljonne, D., Coropceanu, V., & Cornil, J. (2004). Charge-transfer and energy-transfer processes in π-conjugated oligomers and polymers: a molecular picture. Chemical reviews, 104(11), 4971-5004.

[15] Baldo, M. A., O'Brien, D. F., You, Y., Shoustikov, A., Sibley, S., Thompson, M. E., & Forrest, S. R. (1998). Nature1998, 395, 151− 154.

[16] Mizuno, Y., Takasu, I., Uchikoga, S., Enomoto, S., Sawabe, T., Amano, A., ... & Adachi, C. (2012). Fluorinated carbazole derivatives as wide-energy-gap host material for blue phosphorescent organic light-emitting diodes. The Journal of Physical Chemistry C, 116(39), 20681-20687.

[17] Feng, Q., Zhou, Y., Xu, H., Liu, J., Wan, Z., Wang, Y., ... & Huang, H. (2025). BN-embedded aromatic hydrocarbons: synthesis, functionalization and applications. Chemical Society Reviews, 54(12), 5995-6061.

[18] Han, J., Chen, Y., Li, N., Huang, Z., & Yang, C. (2022). Versatile boron-based thermally activated delayed fluorescence materials for organic light-emitting diodes. Aggregate, 3(5), e182.

[19] Hatakeyama, T., Shiren, K., Nakajima, K., Nomura, S., Nakatsuka, S., Kinoshita, K., ... & Ikuta, T. (2016). Ultrapure Blue Thermally Activated Delayed Fluorescence Molecules: Efficient HOMO-LUMO Separation by the Multiple Resonance Effect. Advanced Materials (Deerfield Beach, Fla.), 28(14), 2777-2781.

[20] Chen, X., Tan, D., & Yang, D. T. (2022). Multiple-boron–nitrogen (multi-BN) doped π-conjugated systems for optoelectronics. Journal of Materials Chemistry C, 10(37), 13499-13532.

[21] Liu, B., Cui, J., Wu, X., Zhou, J., Zhang, L., Li, C., & Liu, X. (2026). Bis-BN-embedded [4] helicenes: synthesis, structures and properties. Chemical Communications.

[22] Kotowicz, S., Korzec, M., Pająk, A. K., Golba, S., Małecki, J. G., Siwy, M., & Schab-Balcerzak, E. (2021). New acceptor–donor–acceptor systems based on bis-(Imino-1, 8-Naphthalimide). Materials, 14(11), 2714.

[23] Wang, Z., Li, W., Zhang, J., Zhao, J., Luo, M., Du, S., & Ge, Z. (2023). Carbazole-based thermally activated delayed fluorescent emitters for efficient pure blue organic light-emitting diodes. Organic Electronics, 118, 106795.

[24] Kumar, A., Lenka, S., Patidar, K., Tung, C. A., Luo, M. Y., Beresneviciute, R., & Grigalevicius, S. (2026). Thermally Stable and Energy Efficient Newly Synthesized Bipolar Emitters for Yellow and Green OLED Devices. Molecules, 31(1), 158.

[25] Ledwon, P. (2019). Recent advances of donor-acceptor type carbazole-based molecules for light emitting applications. Organic Electronics, 75, 105422.

[26] Kagatikar, S., & Sunil, D. (2022). A systematic review on 1, 8-naphthalimide derivatives as emissive materials in organic light-emitting diodes. Journal of Materials Science, 57(1), 105-139.

[27] Kotowicz, S., Korzec, M., Małecki, J. G., Golba, S., Siwy, M., Maćkowski, S., & Schab-Balcerzak, E. (2022). Six New Unsymmetrical Imino-1, 8-naphthalimide Derivatives Substituted at 3-C Position—Photophysical Investigations. Materials, 15(19), 7043.

[28] Schab-Balcerzak, E., Siwy, M., Filapek, M., Kula, S., Malecki, G., Laba, K., ... & Domanski, M. (2015). New core-substituted with electron-donating group 1, 8-naphthalimides towards optoelectronic applications. Journal of Luminescence, 166, 22-39.

[29] Zhang, J., He, B., Hu, Y., Alam, P., Zhang, H., Lam, J. W., & Tang, B. Z. (2021). Stimuli-Responsive AIEgens. Advanced Materials, 33(32), 2008071.

[30] Liu, Y., Li, C., Ren, Z., Yan, S., & Bryce, M. R. (2018). All-organic thermally activated delayed fluorescence materials for organic light-emitting diodes. Nature Reviews Materials, 3(4), 18020.

[31] Cao, W., Zhu, X., Li, Q., Yuan, R., & Wang, H. (2023). Intramolecular DA structure achieved excellent electrochemiluminescence of g-C3N4 originated from doping thiophene ring. Chemical Engineering Journal, 475, 146225.

[32] Gaussian 16, Revision C.01, M. J. Frisch, G. W. Trucks, H. B. Schlegel, G. E. Scuseria, M. A. Robb, J. R. Cheeseman, G. Scalmani, V. Barone, G. A. Petersson, H. Nakatsuji, X. Li, M. Caricato, A. V. Marenich, J. Bloino, B. G. Janesko, R. Gomperts, B. Mennucci, H. P. Hratchian, J. V. Ortiz, A. F. Izmaylov, J. L. Sonnenberg, D. Williams-Young, F. Ding, F. Lipparini, F. Egidi, J. Goings, B. Peng, A. Petrone, T. Henderson, D. Ranasinghe, V. G. Zakrzewski, J. Gao, N. Rega, G. Zheng, W. Liang, M. Hada, M. Ehara, K. Toyota, R. Fukuda, J. Hasegawa, M. Ishida, T. Nakajima, Y. Honda, O. Kitao, H. Nakai, T. Vreven, K. Throssell, J. A. Montgomery, Jr., J. E. Peralta, F. Ogliaro, M. J. Bearpark, J. J. Heyd, E. N. Brothers, K. N. Kudin, V. N. Staroverov, T. A. Keith, R. Kobayashi, J. Normand, K. Raghavachari, A. P. Rendell, J. C. Burant, S. S. Iyengar, J. Tomasi, M. Cossi, J. M. Millam, M. Klene, C. Adamo, R. Cammi, J. W. Ochterski, R. L. Martin, K. Morokuma, O. Farkas, J. B. Foresman, and D. J. Fox, Gaussian, Inc., Wallingford CT, 2019.

[33] Dennington, R., Keith, T. A., & Millam, J. M. (2016). GaussView 6.0. 16. Semichem Inc.: Shawnee Mission, KS, USA, 143-150.

[34] Bartolotti, L. J., & Flurchick, K. (1996). An introduction to density functional theory. Reviews in computational chemistry, 187-216.

[35] Engel, E. (2011). Density functional theory. Springer-Verlag Berlin.

[36] Marques, M. A., Maitra, N. T., Nogueira, F. M., Gross, E. K., & Rubio, A. (Eds.). (2012). Fundamentals of time-dependent density functional theory (Vol. 837, p. 130). Berlin, Heidelberg: Springer Berlin Heidelberg.

[37] Becke, A. D. (1988). Density-functional exchange-energy approximation with correct asymptotic behavior. Physical review A, 38(6), 3098.

[38] Lee, C., Yang, W., & Parr, R. G. (1988). Development of the Colle-Salvetti correlation-energy formula into a functional of the electron density. Physical review B, 37(2), 785.

[39] Froitzheim, T., Kunze, L., Grimme, S., Herbert, J. M., & Mewes, J. M. (2024). Benchmarking charge-transfer excited states in TADF emitters: ΔDFT outperforms TD-DFT for emission energies. The Journal of Physical Chemistry A, 128(30), 6324-6335.

[40] Hall, D., Sancho-García, J. C., Pershin, A., Beljonne, D., Zysman-Colman, E., & Olivier, Y. (2023). Benchmarking dft functionals for excited-state calculations of donor–acceptor tadf emitters: Insights on the key parameters determining reverse inter-system crossing. The Journal of Physical Chemistry A, 127(21), 4743-4757.

[41] Mondal, A. (2025). Enhancing the prediction of TADF emitter properties using Δ-machine learning: A hybrid semi-empirical and deep tensor neural network approach. The Journal of Chemical Physics, 162(14).

[42] Cardona, C. M., Li, W., Kaifer, A. E., Stockdale, D., & Bazan, G. C. (2011). Electrochemical considerations for determining absolute frontier orbital energy levels of conjugated polymers for solar cell applications.

[43] Chen, D., & Wang, H. (2019). HOMO–LUMO gaps of homogeneous polycyclic aromatic hydrocarbon clusters. The Journal of Physical Chemistry C, 123(45), 27785-27793.

[44] Bard, A. J., Faulkner, L. R., & White, H. S. (2022). Electrochemical methods: fundamentals and applications. John Wiley & Sons.

[45] Macionis, S., Rashid, E. U., Simokaitiene, J., Butkute, R., Bezvikonnyi, O., Volyniuk, D., & Grazulevicius, J. V. (2025). Effect of bipolar charge transport of derivatives of 1-phenyl-1H-benzo [d] imidazole with horizontal molecular orientation on the performance of OLEDs based on thermally activated delayed fluorescence or phosphorescence. Journal of Materials Chemistry C.

[46] R.G. Pearson, Absolute electronegativity and hardness correlated with molecular orbital theory, Proc. Natl. Acad. Sci. 83 (22) (1986) 8440–8441.

[47] R.G. Parr, R.G. Pearson, Absolute hardness: companion parameter to absolute electronegativity, J. Am. Chem. Soc. 105 (26) (1983) 7512–7516.

[48] T. Koopmans, Über die Zuordnung von Wellenfunktionen und Eigenwerten zuden einzelnen Elektronen eines Atoms, Physica 1 (1–6) (1934) 104–113.

[49] Parr RG, Szentpály LV, Liu S (1999) Electrophilicity index. J Am Chem Soc 121(9):1922–1924.

[50] Gázquez JL, Cedillo A, Vela A (2007) Electrodonating and electroaccepting powers. J Phys Chem A 111(10):1966–1970.

[51] Jia, L., Wu, Q., Yang, T., Xie, B., Sheng, J., Xie, W., & Shi, J. (2025). BN-Doped Polycyclic Aromatic Hydrocarbons and Their Applications in Optoelectronics. Molecules, 30(21), 4252.

[52] Das, S., & Shukla, A. (2026). Tuning the optoelectronic properties of graphene quantum dots by BN-ring doping: A density functional theory study. Physical Review B, 113(7), 075426.

[53] Li, H., Liu, G., & Jiang, Z. (2025). Research progress on multiple resonance thermally activated delayed fluorescence materials featuring red, green, and blue emission based on 1, 4-azaborine. New Journal of Chemistry.

[54] Zhang, Y., Li, W., Jiang, R., Zhang, L., Li, Y., Xu, X., & Liu, X. (2022). Synthetic doping of acenaphthylene through BN/CC isosterism and a direct comparison with BN-acenaphthene. The Journal of Organic Chemistry, 87(19), 12986-12996.

[55] Kim, T. H., Kim, J. H., & Kang, K. (2023). Molecular doping principles in organic electronics: fundamentals and recent progress. Japanese Journal of Applied Physics, 62(SE), SE0803.

[56] Karakuş, N., & Işın, D. Ö. (2025). Optimizing OLED efficiency through thermally activated delayed fluorescence: Computational insights into position isomers of BN-perylenes. Journal of Molecular Graphics and Modelling, 109184.

[57] Mustafa, G., Shafiq, I., Shaikh, Q. U. A., Mustafa, A., Zahid, R., Rasool, F., ... & Haroon, M. (2023). Quantum chemical exploration of A− π1–D1–π2–D2-type compounds for the exploration of chemical reactivity, optoelectronic, and third-order nonlinear optical properties. ACS omega, 8(25), 22673-22683.

[58] Loc, T. H. H., Nhan, N., Thuy, N. P., Ngoc, H. N. B., Nguyen, D. T., & Nhat, P. V. (2026). Effects of substituents on the charge transport properties and nonlinear optical responses of TMCz-BO. Structural Chemistry, 1-14.

[59] Acosta-Quiroga, K., Polo-Cuadrado, E., Percino, M. J., Blanco-Acuña, E., Villaman, D., Pérez-Gutiérrez, E., & Rojas-Peña, C. (2025). Optoelectronic and NLO potential of styryl-functionalized nitroisoxazoles for OLED technologies. Journal of Materials Chemistry C, 13(18), 9083-9098.

[60] CW, T. (1987). Van Slyke S A. Organic electroluminescent diodes Appl Phys Lett, 51, 913-915.

[61] Yadav, R. A. K., Dubey, D. K., Chen, S. Z., Liang, T. W., & Jou, J. H. (2020). The Role of Molecular Orbital Energy Levels in OLED Performance. Scientific reports, 10(1), 9915.

[62] Reineke, S., Thomschke, M., Lüssem, B., & Leo, K. (2013). White organic light-emitting diodes: Status and perspective. Reviews of Modern Physics, 85(3), 1245-1293.

[63] Prabha, K., & Chaya, B. M. (2025). Design, Modelling and Optimization of Nano-Gratings on PHOLEDs for Visible Light Communication. Journal of Electronic Materials, 54(6), 4743-4755.

[64] Uoyama, H., Goushi, K., Shizu, K., Nomura, H., & Adachi, C. (2012). Highly efficient organic light-emitting diodes from delayed fluorescence. Nature, 492(7428), 234-238.

[65] Wong, M. Y., & Zysman-Colman, E. (2017). Purely organic thermally activated delayed fluorescence materials for organic light-emitting diodes. Advanced Materials, 29(22), 1605444.

[66] Li, X. Z., Ye, Y., Cao, Y., Zhang, D., Lin, Y., Chang, J., ... & Wang, J. (2025). Tin-halide perovskites for light-emitting diodes. Chemical Society Reviews.

[67] Jou, J. H., Kumar, S., Agrawal, A., Li, T. H., & Sahoo, S. (2015). Approaches for fabricating high efficiency organic light emitting diodes. Journal of Materials Chemistry C, 3(13), 2974-3002.

[68] Sasaki, T., Hasegawa, M., Inagaki, K., Ito, H., Suzuki, K., Oono, T., ... & Fukagawa, H. (2021). Unravelling the electron injection/transport mechanism in organic light-emitting diodes. Nature communications, 12(1), 2706.

[69] Etherington, M. K., Gibson, J., Higginbotham, H. F., Penfold, T. J., & Monkman, A. P. (2016). Revealing the spin–vibronic coupling mechanism of thermally activated delayed fluorescence. Nature Communications, 7(1), 13680.

[70] Wong, M. Y., & Zysman-Colman, E. (2017). Purely organic thermally activated delayed fluorescence materials for organic light-emitting diodes. Advanced Materials, 29(22), 1605444.